

DEVELOPMENT OF A NOVEL HYBRID UNIFIED VISCOPLASTIC CONSTITUTIVE MODEL

LUIS ALEJANDRO VARELA JIMENEZ

Department of Mechanical Engineering

APPROVED:

Calvin M. Stewart, Ph.D., Chair

Yirong Lin, Ph.D.

David A. Roberson, Ph.D.

Charles Ambler, Ph.D.

Dean of the Graduate School

Copyright ©

by

Luis Alejandro Varela Jimenez

2015

Dedicado a mi familia, a los de aquí y a los que desde arriba siguen aquí.

PREVIEW

DEVELOPMENT OF A NOVEL HYBRID UNIFIED VISCOPLASTIC CONSTITUTIVE MODEL

by

LUIS ALEJANDRO VARELA JIMENEZ, B.S.M.E.

THESIS

Presented to the Faculty of the Graduate School of
The University of Texas at El Paso
in Partial Fulfillment
of the Requirements
for the Degree of
MASTER OF SCIENCE

Department of Mechanical Engineering
THE UNIVERSITY OF TEXAS AT EL PASO

May 2015

UMI Number: 1592006

All rights reserved

INFORMATION TO ALL USERS

The quality of this reproduction is dependent upon the quality of the copy submitted.

In the unlikely event that the author did not send a complete manuscript and there are missing pages, these will be noted. Also, if material had to be removed, a note will indicate the deletion.



UMI 1592006

Published by ProQuest LLC (2015). Copyright in the Dissertation held by the Author.

Microform Edition © ProQuest LLC.

All rights reserved. This work is protected against unauthorized copying under Title 17, United States Code



ProQuest LLC.
789 East Eisenhower Parkway
P.O. Box 1346
Ann Arbor, MI 48106 - 1346

ACKNOWLEDGEMENTS

I would like to thank my advisor Dr. Calvin M. Stewart, whose guidance and advice was fundamental to complete my master degree. It has been an honor to work and learn from such a professional advisor. I want to state my gratitude to the Mechanical Engineering Department for all the opportunities that have been provided to me which have tremendously contributed to my professional career. Finally I would like to thank my family for being my inspiration and for all the provided support.

PREVIEW

ABSTRACT

Gas turbines are now days used in power plants for power generation and for propulsion in the aerospace industry. In these applications gas turbines are exposed to severe temperature and pressure variations during operating cycles. These severe operating conditions exposed the turbine's components to multiple deformation mechanisms which degrade the material and eventually lead to failure of the components. Nickel based and austenitic super alloys are candidate material used for these applications due to its high strength and corrosion resistance at elevated temperatures. At such temperature levels, candidate materials exhibit a rate-dependent or viscoplastic behavior which difficult the prediction or description of the material response due to deformation mechanisms. Unified viscoplastic constitutive models are used to describe this viscoplastic behavior of materials. In the present work Miller and Walker unified viscoplastic models are presented, described and exercised to model the creep of Hastelloy X and the low cycle fatigue behavior of stainless steel 304. The numerical simulation results are compared to an extensive database of experimental data to fully validate the capabilities and limitations of the considered models. Material constant heuristic optimizer (MACHO) software is explained and used to determine both models material constants and ensure a systematic calculation of them. This software uses the simulated annealing algorithm to determine the optimal material constants values in a global surface, by comparing numerical simulations to an extensive database of experimental data. A quantitative analysis on the performance of both models is conducted to determine the most suitable model to predict material's behavior. Based on the two exercised classical viscoplastic models, a novel hybrid unified model is introduced, to accurately describe the inelastic behavior caused by creep and fatigue effects at high temperature. The presented

hybrid model consists on the combination of the best aspects of Miller and Walker model constitutive equations, with the addition of a damage rate equation which provides capabilities to describe damage evolution and life prediction for Hastelloy X and stainless steel 304. A detailed explanation on the meaning of each material constant is provided, along with its impact on the hybrid model behavior. To validate the capabilities of the proposed hybrid model, numerical simulation results are compared to a broad range of experimental data at different stress levels and strain rates; besides the consideration of two alloys in the present work, would demonstrate the model's capabilities and flexibility to model multiple alloys behavior. Finally a quantitative analysis is provided to determine the percentage error and coefficient of determination between the experimental data and numerical simulation results to estimate the efficiency of the proposed hybrid model.

TABLE OF CONTENTS

| | |
|---|------|
| ACKNOWLEDGEMENTS | v |
| ABSTRACT | vi |
| TABLE OF CONTENTS | viii |
| LIST OF TABLES | xi |
| LIST OF FIGURES | xiii |
| CHAPTER 1: INTRODUCTION | 1 |
| 1.1 MOTIVATION | 1 |
| 1.2 OBJECTIVE | 9 |
| 1.3 OUTLINE | 10 |
| CHAPTER 2: BACKGROUND | 11 |
| 2.1 FUNDAMENTALS OF VISCOPLASTICITY | 11 |
| 2.2 MILLER MODEL | 15 |
| 2.2.1 MILLER MODEL EQUATIONS | 16 |
| 2.2.2 MATERIAL CONSTANTS | 18 |
| 2.3 WALKER MODEL | 21 |
| 2.3.1 WALKER MODEL EQUATIONS | 22 |

| | |
|---|----|
| 2.3.2 MATERIAL CONSTANTS | 24 |
| 2.4 MATERIAL DAMAGE | 25 |
| 2.4.1 KACHANOV CREEP DAMAGE MODEL | 25 |
| 2.4.2 SIN-HYPERBOLIC CREEP DAMAGE MODEL | 27 |
| CHAPTER 3: MATERIALS | 28 |
| 3.1 HASTELLOY X | 28 |
| 3.2 STAINLESS STEEL 304 | 29 |
| CHAPTER 4: NUMERICAL OPTIMIZATION SOFTWARE | 30 |
| 4.1 OPTIMIZATION PROCESS | 31 |
| 4.2 OPTIMIZATION PARAMETERS | 35 |
| CHAPTER 5: EXERCISE OF MILLER AND WALKER MODELS | 36 |
| 5.1 OPTIMIZED MATERIAL CONSTANTS | 36 |
| 5.2 RESULTS | 44 |
| 5.3 ANALYSIS | 58 |
| CHAPTER 6: DEVELOPMENT AND EXERCISE OF A NOVEL HYBRID UNIFIED VISCOPLASTIC MODEL | 62 |
| 6.1 HYBRID MODEL V0 | 62 |
| 6.1.1 MODEL DEVELOPMENT | 63 |
| 6.1.2 EXERCISE OF HYBRID MODEL V0 | 64 |

| | |
|---|-----|
| 6.2 HYBRID MODEL V1 | 71 |
| 6.2.1 MODEL DEVELOPMENT | 71 |
| 6.2.2 EXERCISE OF HYBRID MODEL V1 | 73 |
| 6.3 HYBRID MODEL V2 | 81 |
| 6.3.1 MODEL DEVELOPMENT | 81 |
| 6.3.2 EXERCISE OF HYBRID MODEL V2 | 82 |
| CHAPTER 7: CONCLUSION & FUTURE WORK | 94 |
| 7.1 CONCLUSIONS | 94 |
| 7.2 FUTURE WORK | 97 |
| REFERENCES | 98 |
| APPENDIX | 105 |
| APPENDIX 1: HYBRID MODEL V2 UPF | 105 |
| VITA | 109 |

LIST OF TABLES

| | |
|---|----|
| Table 1: Hastelloy X chemical composition (weight. %) [32] | 28 |
| Table 2: stainless steel 304 chemical composition (weight. %) [68]..... | 29 |
| Table 3: Miller model initial guess and optimized material constants for Hastelloy X creep..... | 38 |
| Table 4: Walker model initial guess and optimized material constants for Hastelloy X creep | 39 |
| Table 5: Miller model initial guess and optimized material constants for stainless steel 304..... | 43 |
| Table 6: Walker model initial guess and optimized material constants for stainless steel 304 | 43 |
| Table 7: Calculated mean percentage error (MPE) and coefficient of determination R^2 for Miller and Walker numerical simulations for Hastelloy X subjected to creep..... | 60 |
| Table 8: Calculated mean percentage error (MPE) and coefficient of determination R^2 for Miller and Walker numerical simulations for stainless steel 304 subjected to low cycle fatigue | 61 |
| Table 9: Hastelloy X creep material constants for hybrid model V0 | 64 |
| Table 10: 304 Stainless steel low cycle fatigue material constants for hybrid model V0 | 65 |
| Table 11: Mean percentage error (MPE) and coefficient of determination (R^2) of Hastelloy X creep simulations hybrid model V0 | 69 |
| Table 12: Mean percentage error (MPE) and coefficient of determination (R^2) of 304 stainless steel data low cycle fatigue simulations hybrid model V0 | 70 |
| Table 13: Rest stress rate equations tested for improvement..... | 72 |
| Table 14: Hastelloy X Creep Material Constants for hybrid model V1 | 73 |
| Table 15: Stainless Steel 304 Fatigue Material Constants for hybrid model V1 | 74 |
| Table 16: Mean percentage error (MPE) and coefficient of determination (R^2) of Hastelloy X creep simulations hybrid model V1 | 79 |

| | |
|--|----|
| Table 17: Mean percentage error (MPE) and coefficient of determination (R^2) of 304 stainless steel data low cycle fatigue simulations hybrid model V1 | 80 |
| Table 18: Hastelloy X creep material constants for hybrid model V2 | 83 |
| Table 19: 304 Stainless Steel Fatigue material constants for hybrid model V2 | 84 |
| Table 20: Mean percentage error (MPE) and coefficient of determination (R^2) of Hastelloy X data creep simulations hybrid model V2 | 92 |
| Table 21: Mean percentage error (MPE) and coefficient of determination (R^2) of 304 stainless steel data low cycle fatigue simulations hybrid model V2 | 93 |

PREVIEW

LIST OF FIGURES

| | |
|---|----|
| Figure 1: NGNP configuration 1 (direct electrical cycle and a parallel IHX) | 2 |
| Figure 2: NGNP configuration 2 (direct electrical cycle, parallel IHX, and SHX)..... | 3 |
| Figure 3: NGNP configuration 3 (indirect electrical cycle and a parallel SHX) | 3 |
| Figure 4: Gas turbine Alstom GT24/26 [10]..... | 5 |
| Figure 5: W501 F Gas turbine components (a) combustor, (b) transition pieces, (c) Alstom GT24/26 rotating gas turbine blades and (d) exhaust components [10],[19] | 6 |
| Figure 6: Failure of turbine components [24],[25]..... | 7 |
| Figure 7: Effects of constants C1, H1 and C2. | 19 |
| Figure 8: Stress-strain behavior at high n1 and n2 values | 24 |
| Figure 9: MACHO material constant optimization process | 34 |
| Figure 10: Objective Function results of the optimization process of Miller and Walker models for Hastelloy X under creep..... | 37 |
| Figure 11: Objective function results of the optimization process of Miller and Walker models for 304 stainless steel under fatigue..... | 42 |
| Figure 12: Miller model simulation vs. experimental data [32] | 48 |
| Figure 13: Miller model drag stress vs. time | 48 |
| Figure 14: Miller model rest stress vs. time..... | 49 |
| Figure 15: Walker model simulation vs. experimental data [32]..... | 49 |
| Figure 16: Walker model drag stress vs. time..... | 50 |
| Figure 17: Walker model rest stress vs. time..... | 50 |
| Figure 18: Miller model simulation vs. experimental data [68] | 52 |
| Figure 19: Miller model simulation vs. experimental data [68] | 52 |

| | |
|---|----|
| Figure 20: Walker model simulation vs. experimental data [68]..... | 54 |
| Figure 21: Walker model simulation vs. experimental data [68]..... | 54 |
| Figure 22: Comparison of stress amplitude vs. number of cycles at $\Delta\epsilon=0.005$ | 57 |
| Figure 23: Comparison of stress amplitude vs. number of cycles at $\Delta\epsilon=0.007$ | 57 |
| Figure 24: Hastelloy X creep vs hybrid model V0 simulation at multiple stress levels..... | 67 |
| Figure 25: 304 Stainless steel low cycle fatigue vs. hybrid model V0 simulation at $\Delta\epsilon=0.005$... | 68 |
| Figure 26: 304 Stainless steel low cycle fatigue vs. hybrid model V0 simulation at $\Delta\epsilon=0.007$... | 68 |
| Figure 27: Hastelloy X creep experimental data vs. Hybrid model V1 simulated data..... | 75 |
| Figure 28: Hastelloy X creep experimental data vs. Hybrid model V1 simulated data..... | 76 |
| Figure 29: Stainless Steel 304 experimental data vs. Hybrid model V1 simulated data. | 77 |
| Figure 30: Stainless Steel 304 experimental data vs. Hybrid model V1 simulated data. | 78 |
| Figure 31: Hastelloy X creep experimental data vs. Hybrid model V2 simulated data..... | 86 |
| Figure 32: Hastelloy X creep experimental data vs. Hybrid model V2 simulated data..... | 86 |
| Figure 33: Stainless Steel 304 experimental data vs. Hybrid model V2 simulated data. | 88 |
| Figure 34: Stainless Steel 304 experimental data vs. Hybrid model V2 simulated data. | 89 |
| Figure 35: Comparison of stress amplitude and number of cycles at $\Delta\epsilon=0.005$ | 91 |
| Figure 36: Comparison of stress amplitude and number of cycles at $\Delta\epsilon=0.007$ | 91 |

CHAPTER 1: INTRODUCTION

1.1 MOTIVATION

Nuclear and chemical reactors are now being used to generate electricity with clean methods without the emission of greenhouse gases [1]. Some examples of these types of reactors are: the Very-High Temperature Reactor (VHTR) which is the Next Generation Nuclear Plant (NGNP) in the United States [2], the High Temperature Test Reactor (HTTR) in Japan [3], Nuclear Hydrogen Development and Demonstration plant in Korea [4], and the High temperature Gas Reactor in Japan [5]. The efficiency of these reactors is related to the temperature at which they operate; therefore, high operating temperatures are desired for better efficiencies. During operation at high temperature, the reactor requires cooling systems to keep it within safe operating temperature ranges. The coolant system is formed by the intermediate heat exchanger (IHX), which exchange heat between the primary heated coolant that come directly from the reactor primary system to a secondary working fluid which cools down the primary coolant [1-3]. Three design configuration recommended by Davis et al. [6] for NGNP are presented in Figure 1-Figure 3 [7]. NGNP proposed configuration 1 is presented in Figure 1, this configuration requires the smallest IHX design and produces the highest overall electrical power production efficiency for the NGNP. In the design configuration 1, the designed operating conditions are: reactor outlet temperature is in the range of 850°C - 950°C, the IHX inlet pressure of 7.0 MPa and outlet pressure of 6.95 MPa, IHX inlet temperature is 850°C - 950°C and outlet temperature of 523°C – 628°C. Proposed configuration 2 is presented in Figure 2; this configuration is similar to configuration 1, but includes a third loop which adds a separation between the NGNP and a hydrogen generation process. In the design configuration 2 the reactor

outlet temperature is in the range of 900°C – 950°C, with IHX inlet pressure of 7.0 MPa and outlet pressure of 6.95 MPa, IHX inlet temperature is 900°C – 950°C and outlet temperature of 543°C-593°C. Finally the design configuration 3 is presented in Figure 3; this configuration requires the larger IHX design since it must transfer all the reactor thermal power to the external power conversion system and hydrogen generation process. In design configuration 3 the reactor outlet temperature is in the range of 950°C – 950°C, IHX inlet pressure of 7.0 MPa and outlet pressure of 6.95MPa, IHX inlet temperature of 850°C – 950°C and outlet temperature of 484°C - 584°C [7].

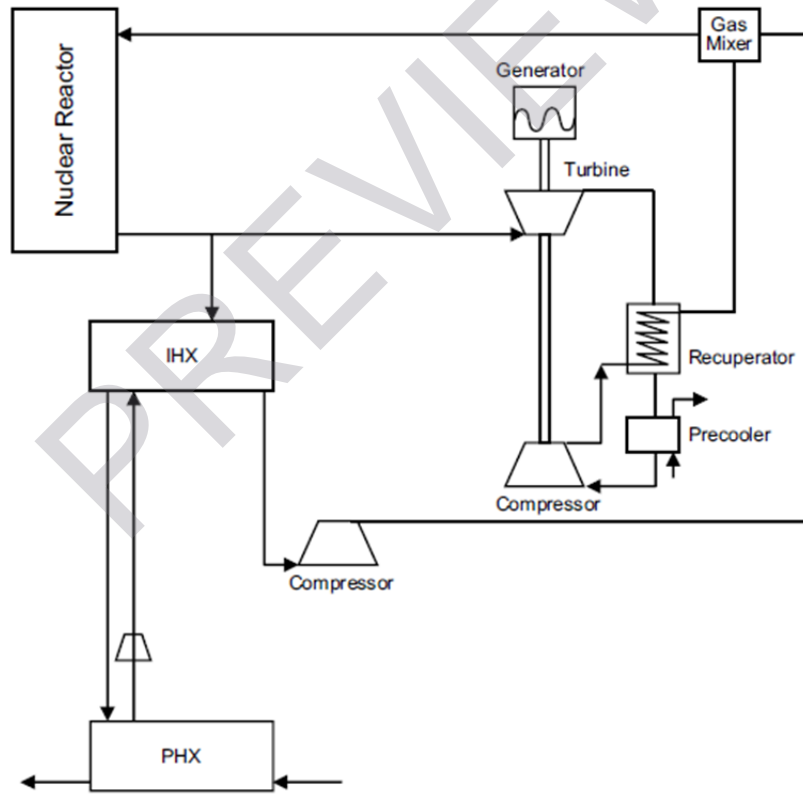


Figure 1: NGNP configuration 1 (direct electrical cycle and a parallel IHX)

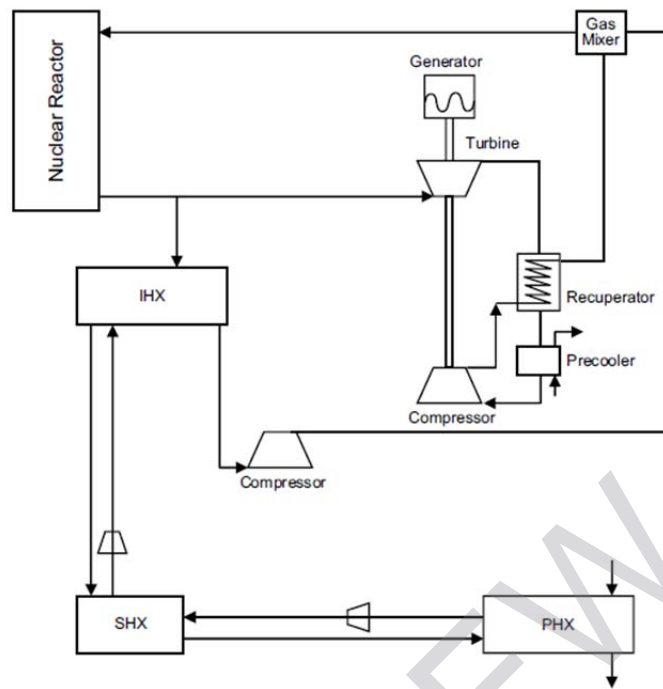


Figure 2: NGNP configuration 2 (direct electrical cycle, parallel IHX, and SHX)

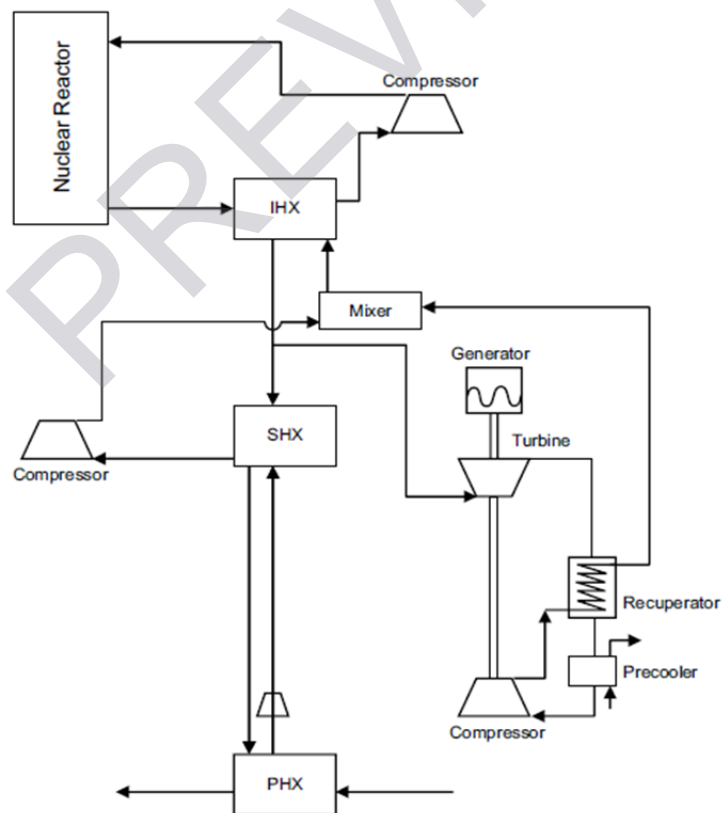


Figure 3: NGNP configuration 3 (indirect electrical cycle and a parallel SHX)

From the previous described design configurations, it can be observed how in configuration 1 the IHX operates at higher temperatures; thus, resulting in the most efficient configuration for the NGNP plant, meaning that the higher the operating temperature the higher efficiencies the system results on. Hence, the IHX perform a crucial function and its optimal performance is vital to maintain a safe temperature and a high efficiency of the reactor; consequently, accurate IHX piping component design is pivot to achieve high quality designs of IHX piping. Therefore it is essential to have a deep understanding of the mechanical behavior of the constituent material used in the components under service-like conditions [8]. Since the IHX is operating at high temperature and extreme conditions, a material able to deal with thermal and mechanical stresses, corrosion, oxidation, and exhibit a high strength at elevated temperature is required for IHX piping components.

Gas turbines are extensively used for generation of electricity in power plants, and for propulsion in aerospace industry [9] (Figure 4). This kind of turbo machinery operates at elevated temperatures of above 1100°C, and high pressure ratios of up to 23 to 1 for periods of more than 25,000 hours [11-13]. The Thermomechanical efficiency of gas turbines is dependent on the temperature at which the turbine operates. A high firing temperature leads to a dual benefit, an increase in specific work (that is the output per unit of air flow), and a reduction in fuel consumption [14-17]. These severe operation conditions produce multiple deformation mechanisms, which are applied to the turbine components such as the combustors, transition pieces, exhaust, and turbine blades [13, 18] illustrated in Figure 5. The purpose of the combustor is to mix the compressed air coming from the compressor with the fuel, and ignite the air-fuel mixture at temperatures of above 1500°C. An example of a gas turbine combustor is provided in Figure 5 (a).

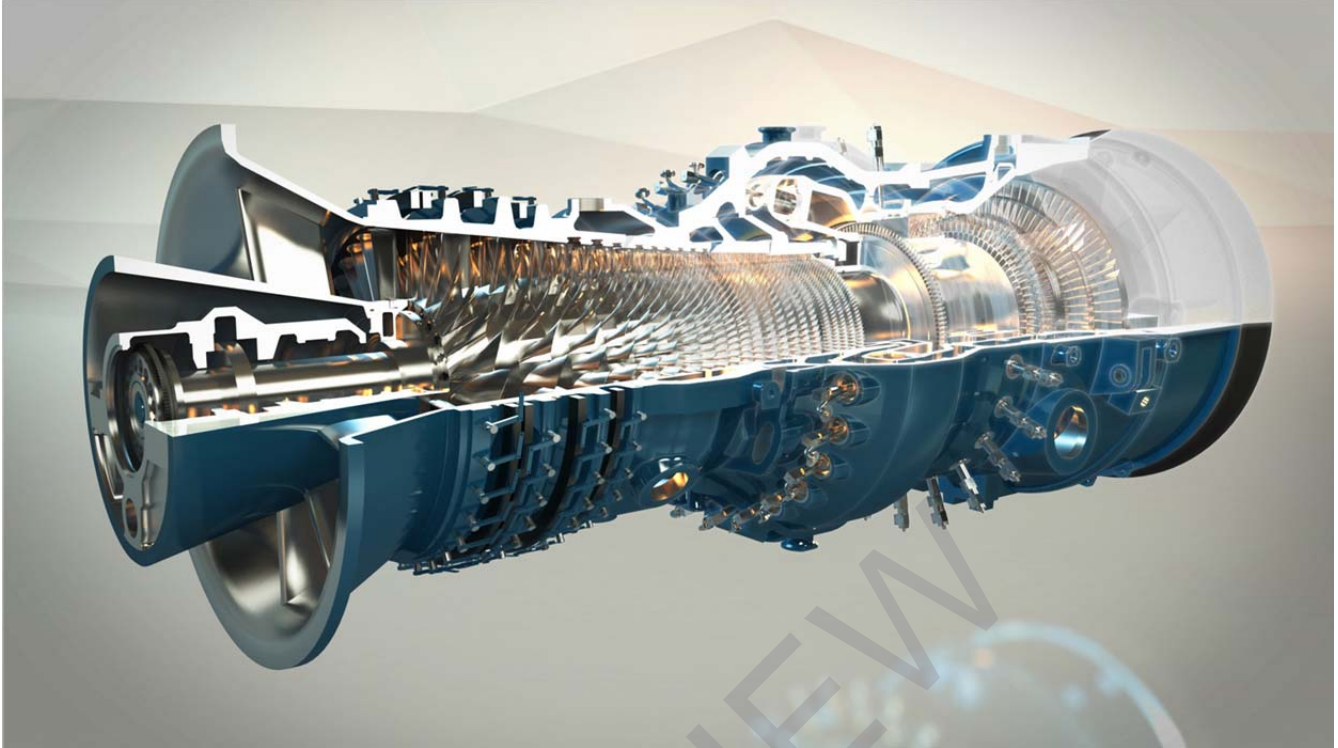


Figure 4: Gas turbine Alstom GT24/26 [10]

After the combustion process is done the combustion gases left the combustor and then enter the transition pieces which direct the gases against the nozzle guide vanes. An example of transition pieces is given in Figure 5 (b). The purpose of the nozzle guide vanes is to direct the combustion gasses to intersect the rotating turbine blades at the optimum angle. An example of rotating turbine blades is presented in Figure 5 (c). These components capture the combustion gases momentum causing the rotor to spin therefore generating power, Figure 5 (d) shows an example of exhaust components, which are responsible of directing the combustion gases out of the turbine once they passed through all the rotating turbine blades rows [20]. Some damage mechanisms are thermal stresses which are caused by the elevated operational temperature; mechanical stresses caused by the pressure differences and the rotational movement of components, creep which is caused by the long operation periods of the turbine, low and high



(a)



(b)



(c)



(d)

Figure 5: W501 F Gas turbine components (a) combustor, (b) transition pieces, (c) Alstom GT24/26 rotating gas turbine blades and (d) exhaust components [10],[19]

cycle fatigue caused by vibrations, the start-up , service time and shut-down of the equipment, oxidation caused by the contact of components to oxygen during operation. Depending on the damage stage caused by the mentioned mechanisms, they could lead to failure of the gas turbine components [21- 23], which might be catastrophic as shown in Figure 6. The severe operation conditions of gas turbines create a situation where material selection for components' design

plays a fundamental role to warranty components reliability. High strength materials are necessary to provide long components' life under elevated temperature [26-28].



Figure 6: Failure of turbine components [24],[25]

For the previously described applications (IHX and gas turbine applications) good material candidates are austenitic, hardened superalloys [29]. The nickel-based superalloy Hastelloy X is an attractive candidate material. It is favored for these applications because of its high nickel content, which provides it with excellent mechanical properties at high temperature, high resistance to creep, oxidation and corrosion. A second candidate material for these type of applications is the austenitic stainless steel 304, which also possess high strength at elevated temperature [30-37]. However at elevated temperature these superalloys exhibit a viscoplastic (rate-dependent) behavior [38]. The nonlinear (viscoplastic) behavior of the material difficult the prediction of the material's response to loading.

In order to have an optimal design of gas turbine and IHX components, a detailed modeling of the material's behavior under any loading condition is essential to ensure the design integrity and quality of the component. Moreover, by knowing the behavior of the material the operational temperature might be increased for better system efficiencies. On the other hand, a better understanding of the material behavior leads to less conservative designs which in return reduce

the cost of hardware and components, since the material is effectively used [15-17, 39]. There has been considerable effort to develop unified constitutive models capable of describing the inelastic behavior of Hastelloy X and stainless steel 304. These “unified” models are designed to model the multiple deformation mechanisms present during various loading cases such as stress relaxation, monotonic tension, creep and fatigue. Historically, numerous viscoplastic models have been proposed in literature such as Chaboche, Bodner, Hart, Miller, Walker, Bodner-Partom among many others [40-44]. Viscoplastic constitutive models are shaped by material constants, which are characteristic of each material. Material constants are typically calculated using specific types of experimental data. The complexity of the model equations and the considered temperature ranges dictates the total number of material constants required for each model. The procedure to calculate these material constants is not well documented leaving gaps in the calculation process that leads to the “unsystematic” calculation of material constants. This unsystematic calculation of constants might result in improper usage of viscoplastic models.